Low-Complexity Adaptive Direct-State Kalman Filter for Robust GNSS Carrier Tracking

Iñigo Cortés*†, Natalia Conde*, J. Rossouw van der Merwe*, Elena Simona Lohan†, Jari Nurmi†, and Wolfgang Felber*

* Fraunhofer Institute for Integrated Circuits IIS, Nuremberg, Germany inigo.cortes@iis.fraunhofer.de

† Tampere University, Electrical Engineering Unit, Tampere, Finland

***Abstract*— This paper evaluates the implementation of a low-complexity adaptive direct-state Kalman filter (DSKF) for robust carrier phase tracking of global navigation satellite system (GNSS) signals. This architecture consists of a loop-bandwidth control algorithm (LBCA)-based lookup table (LUT)-DSKF in an FLL-assisted-PLL (FAP) tracking scheme. The FAP considers the carrier phase and frequency Doppler measurements to achieve a robust tracking. The use of the DSKF in the FAP achieves optimal performance, assuming a known Gaussian distributed model of the states and the measurements. However, the performance decays in time-varying scenarios where the measurements' distribution changes due to noise, signal dynamics, multi-path, and non-line-of-sight effects. In addition, the DSKF's implementation in real-time applications requires a high computational cost. This study derives the so-called LUT-DSKF for the FAP, a simplified DSKF that considers the convergence of the Kalman gains. In addition, the LBCA is used to adapt the time of response of this architecture and improve the tracking performance in time-varying scenarios. The presented technique is compared with the adaptive LUT-DSKF in a phase-locked loop (PLL) tracking scheme. These two tracking architectures are implemented in an open software interface GNSS hardware receiver. The receiver is evaluated in simulated scenarios with different dynamics and noise cases for each implementation. The results confirm that the LBCA-based LUT-DSKF in the FAP exhibits superior dynamic tracking performance than the adaptive PLL while maintaining similar static tracking performance and low complexity.**

***Index Terms*—Global navigation satellite system (GNSS), FLL-assisted-PLL (FAP), lookup table (LUT)-direct-state Kalman filter (DSKF), discrete algebraic Riccati equation (DARE), loop-bandwidth control algorithm (LBCA).**

I. Introduction

Synchronization is the key component of global navigation satellite system (GNSS) receivers. It consists of two stages: acquisition and tracking. Acquisition coarsely estimates the code phase and carrier Doppler of incoming GNSS signals. The tracking stage refines these synchronization parameters and includes the fine estimation of the carrier phase. A successful synchronization permits the decoding of the navigation message and the estimation of the pseudo-range and pseudo-range rate, which finally leads to the position, velocity, and time (PVT) calculation.

The scalar tracking loop (STL) is the standard tracking scheme used in the tracking stage. This tracking scheme synchronizes with a single synchronization parameter of an incoming GNSS signal [1], [2]. There are three parameters in a GNSS signal in which the GNSS receiver must synchronize with: the carrier phase ϕ, the carrier Doppler f_{d}, and the code phase τ. Therefore, a tracking channel is composed of three STLs: phase-locked loop (PLL), frequency locked loop (FLL), and delay locked loop (DLL). The STL contains a correlator, a discriminator, a loop filter, and a numerically controlled oscillator (NCO) [2], [3]. The configuration parameters of the STL are the type of discriminator, the loop bandwidth B, the integration time τ_{int}, the order p, and the correlator spacing. These parameters determine the robustness against noise and signal dynamics. The well-known trade-off between noise filtering capabilities and signal dynamics resistance is the main problem of techniques with fixed configurations. In particular, this problem is aggravated in time-varying scenarios. These scenarios are characterized by different realizations of signal dynamics, noise, and fading effects that lead to challenges regarding the synchronization capability [1]. For instance, a high-order STL with wide loop bandwidth and short integration time is adequate to track rapidly changing parameters. In contrast, a low-order STL with narrow loop bandwidth and long integration time is preferable to track noisy parameters. Therefore, a fixed configuration of the STL is not an adequate solution for time-varying scenarios.

The Kalman filter (KF) is an optimal infinite impulse response (IIR) estimator under the assumption of linear Gaussian error statistics [4]–[6]. Good knowledge of the process noise covariance $\mathbf{Q}$ and measurement noise covariance $\mathbf{R}$ allows the KF to optimally adapt its coefficients to achieve the minimum mean square error (MMSE) [7]. There are several KF implementation methods in STLs [8] grouped into error-state Kalman-filter (ESKF) and direct-state Kalman filter (DSKF) [9]. The former replaces the loop filter of the STL with a KF [10]–[13], whereas the latter considers the whole STL as part of the KF [14]–[17]. The implementation of the DSKF is straightforward due to the relation between the STL's coefficients and the DSKF's Kalman gains [14].

The MMSE is only achieved if á priori knowledge of $\mathbf{Q}$ and $\mathbf{R}$ is available or if these are accurately estimated [7]. If this is not the case, the KF converges to a suboptimal solution [18]. Hence, for time-varying scenarios in which $\mathbf{Q}$ and $\mathbf{R}$ continuously change, both the DSKF and STL share the same challenge in synchronization capability.

There has been significant research towards robust tracking solutions to solve this problem [19]. However, there is still ample investigation to find the best technique in terms of performance and complexity [15], [20]. Adaptive tracking

methods can improve the tracking performance in time-varying scenarios. Different methods to estimate the noise covariances of the KF have been summarized in a review study [21]. One solution can be to implement a moving average filter to estimate $\mathbf{Q}$ and $\mathbf{R}$, and consequently adapt optimally the response time of the KF [22]. Moreover, it is possible to implement a carrier-to-noise density ratio (C/N_0)-based DSKF, in which $\mathbf{R}$ depends on the variance of the STL discriminator's output [16]. $\mathbf{Q}$ can also be adapted according to the dynamic stress error [17]. Recent research shows the implementation of a loop-bandwidth control algorithm (LBCA)-based PLL-DSKF [14]. The LBCA performs a loop bandwidth-dependent weighted difference between estimated noise and estimated dynamics of the discriminator's output [23]. The LBCA updates the loop bandwidth and, in turn, $\mathbf{Q}$, based on their steady-state relationship.

Despite the tracking performance advantage of the KF, its implementation in real-time applications requires a high computational cost compared to the STL. Therefore, efficient low-complexity methods have been studied [13], [15]. The complexity of the ESKF can be reduced by taking advantage of the Kalman gains' convergence in the steady state [13]. The same can be done for the DSKF, leading to the so-called lookup table (LUT)-DSKF [15]. The implementation of an LBCA-based LUT-DSKF in a PLL tracking scheme has been presented recently [15]. The ratio between the steady-state process variance and the measurement variance provides a one-to-one relationship between the steady-state Kalman gains and the loop bandwidth. Hence, the LBCA can adapt the loop bandwidth to, in turn, adapt the steady-state Kalman gains.

The aiding of the FLL in the PLL can improve significantly the robustness to high signal dynamics. Recent research presents the implementation of a LBCA-based FLL-assisted-PLL (FAP) architecture [24]. This adaptive tracking architecture consists of two independent LBCAs to adapt the bandwidths of a second-order FLL and a third-order PLL. Although good results have been achieved, extensive tuning was required to find the optimal weighting functions for each LBCA. Also, two LBCAs implied doubled complexity.

This paper presents the implementation of an adaptive LUT-DSKF in a FAP tracking architecture. The derivation of the discrete algebraic Riccati equation (DARE) in the DSKF presents an inter-dependency between FLL and PLL coefficients. The main novelty of this research is the implementation of a single LBCA to adapt the LUT-DSKF's response time based on the found inter-dependency. This inter-dependant factor is the ratio between the steady-state process variance q_a and the carrier phase measurement variance R_ϕ. The LBCA updates this ratio to change the LUT-DSKF's response time. The adaptive LUT-DSKF in the FAP tracking scheme is compared with the adaptive LUT-DSKF in the PLL [15]. Both methods are implemented in the carrier phase synchronization tracking stage of the GOOSE© receiver [25]. Each adaptive technique's tracking performance is evaluated under simulated scenarios with different dynamics and noise levels.

The rest of the paper is organized as follows: Section II describes the DSKF in the FAP tracking scheme, presents the system model, the measurement model, and the state space model (SSM) representation, analyzes the steady-state convergence and derives the tracking scheme of the LUT-DSKF. Section III shows the architecture of the LBCA-based LUT-DSKF. Section IV presents the experimental setup and the achieved results. Finally, Section V concludes and indicates future work.

II. DSKF IN FLL-ASSISTED-PLL ARCHITECTURE

This section describes the DSKF in the FAP tracking scheme of a GNSS receiver. First, the system and measurement models are presented. Next, the KF equations are described, the SSM representation is defined and the transfer function is analyzed. Finally, the LUT-DSKF is derived by solving the DARE.

A. System and Measurement Model

Assuming a Brownian motion model for the acceleration state [26] and based on the backward Euler transform (BET) [27], [28], the discrete system model of the DSKF is represented as:

$$\underbrace{\begin{bmatrix}\phi[n]\\ f[n]\\ a[n]\end{bmatrix}}_{\mathbf{x}[n]} = \underbrace{\begin{bmatrix}1 & \tau_{\text{int}} & \tau_{\text{int}}^2\\ 0 & 1 & \tau_{\text{int}}\\ 0 & 0 & 1\end{bmatrix}}_{\mathbf{A}} \underbrace{\begin{bmatrix}\phi[n-1]\\ f[n-1]\\ a[n-1]\end{bmatrix}}_{\mathbf{x}[n-1]} + \underbrace{\begin{bmatrix}\tau_{\text{int}} & \tau_{\text{int}}^2 & \tau_{\text{int}}^3\\ 0 & \tau_{\text{int}} & \tau_{\text{int}}^2\\ 0 & 0 & \tau_{\text{int}}\end{bmatrix}}_{\mathbf{G}} \underbrace{\begin{bmatrix}0\\ 0\\ w_a[n]\end{bmatrix}}_{\mathbf{w}[n]} \tag{1}$$

where n is the sample index, ϕ is the carrier phase, f is the carrier Doppler, a is the angular acceleration, τ_{int} is the integration time, and w_a is the zero-mean Gaussian distributed perturbation that suffers the acceleration in cycles/s^3. $\mathbf{x}$ is the state vector, $\mathbf{A}$ is the discrete state matrix, and the term $\mathbf{Gw}$ determines the discrete process noise that drives the signal dynamics.

The process covariance matrix $\mathbf{Q}$ is defined as:

$$\mathbf{Q} = \mathbf{G}\,\mathrm{E}[\mathbf{w}\mathbf{w}^{\mathrm{T}}]\,\mathbf{G}^{\mathrm{T}} \tag{2}$$

$$= \mathbf{G}\begin{bmatrix}0 & 0 & 0\\ 0 & 0 & 0\\ 0 & 0 & q_a\end{bmatrix}\mathbf{G}^{\mathrm{T}} \tag{3}$$

$$= q_a\begin{bmatrix}\tau_{\text{int}}^6 & \tau_{\text{int}}^5 & \tau_{\text{int}}^4\\ \tau_{\text{int}}^5 & \tau_{\text{int}}^4 & \tau_{\text{int}}^3\\ \tau_{\text{int}}^4 & \tau_{\text{int}}^3 & \tau_{\text{int}}^2\end{bmatrix} \tag{4}$$

where q_a is the variance of the random process w_a in cycles^2/s^6.

The measurement model is as follows:

$$\underbrace{\begin{bmatrix}z_\phi[n]\\ z_f[n]\end{bmatrix}}_{\mathbf{z}[n]} = \underbrace{\begin{bmatrix}1 & 0 & 0\\ 0 & 1 & 0\end{bmatrix}}_{\mathbf{H}}\mathbf{A}\mathbf{x}[n-1] + \underbrace{\begin{bmatrix}v_\phi\\ v_f\end{bmatrix}}_{\mathbf{v}[n]} \tag{5}$$

where z_ϕ and z_f are the carrier phase and frequency Doppler measurements, and v_ϕ and v_f are the zero-mean Gaussian distributed noise of z_ϕ and z_f. $\mathbf{H}$ defines the measurement model matrix, $\mathbf{z}$ describes the measurement vector, and $\mathbf{v}$ represents the measurement noise vector.

The measurement covariance matrix $\mathbf{R}$ is:

$$\mathbf{R} = \mathrm{E}\left[\mathbf{z}\mathbf{z}^{\mathrm{T}}\right] = \begin{bmatrix} R_\phi & 0 \\ 0 & R_f \end{bmatrix} \tag{6}$$

where R_ϕ and R_f are the variances of v_ϕ and v_f.

B. Kalman Filter Algorithm

The KF is divided into two stages: prediction and update. The prediction step estimates the predicted state $\hat{\mathbf{x}}[n]$ and predicted error covariance $\hat{\mathbf{P}}[n]$. These predictions are calculated based on the previous updated state $\mathbf{x}[n-1]$, the previous updated error covariance $\mathbf{P}[n-1]$ and $\mathbf{Q}$:

$$\hat{\mathbf{x}}[n] = \mathbf{A}\,\mathbf{x}[n-1] \tag{7}$$

$$\hat{\mathbf{P}}[n] = \mathbf{A}\,\mathbf{P}[n-1]\,\mathbf{A}^{\mathrm{T}} + \mathbf{Q}[n] \tag{8}$$

The dimension of the presented variables depends on the KF's state order p: $\{\mathbf{x},\, \hat{\mathbf{x}}\} \in \mathbb{R}^{p\times 1}$, $\left\{\mathbf{A},\, \hat{\mathbf{P}},\, \mathbf{P},\, \mathbf{Q}\right\} \in \mathbb{R}^{p\times p}$.

The update stage determines the updated states $\mathbf{x}[n]$ based on $\hat{\mathbf{x}}[n]$, the measurement residual $\delta\mathbf{z}[n]$ and the Kalman gains $\mathbf{K}$. $\delta\mathbf{z}$ is the difference between $\mathbf{z}[n]$ and the estimated measurement $\widetilde{\mathbf{z}}[n]$ that is calculated based on $\hat{\mathbf{x}}[n]$. $\mathbf{K}$ weights $\delta\mathbf{z}[n]$ and depends on $\hat{\mathbf{P}}[n]$ and $\mathbf{R}[n]$:

$$\delta\mathbf{z}[n] = \mathbf{z}[n] - \mathbf{H}\,\hat{\mathbf{x}}[n] = \mathbf{z}[n] - \widetilde{\mathbf{z}}[n] \tag{9}$$

$$\mathbf{S}[n] = \mathbf{H}\,\hat{\mathbf{P}}[n]\,\mathbf{H}^{\mathrm{T}} + \mathbf{R}[n] \tag{10}$$

$$\mathbf{K}[n] = \hat{\mathbf{P}}[n]\,\mathbf{H}^{\mathrm{T}}\,\mathbf{S}^{-1}[n] \tag{11}$$

$$\mathbf{x}[n] = \hat{\mathbf{x}}[n] + \mathbf{K}[n]\,\delta\mathbf{z}[n] \tag{12}$$

$$\mathbf{P}[n] = (\mathbf{I} - \mathbf{K}[n]\,\mathbf{H}[n])\,\hat{\mathbf{P}}[n] \tag{13}$$

where $\mathbf{S}[n]$ is the innovation covariance matrix, and $\mathbf{I}$ is the identity matrix. The order p and the number of measurements m determine the dimension of the presented variables: $\{\delta\mathbf{z},\, \mathbf{z},\, \widetilde{\mathbf{z}}\} \in \mathbb{R}^{m\times 1}$, $\{\mathbf{S},\, \mathbf{R}\} \in \mathbb{R}^{m\times m}$, $\mathbf{K} \in \mathbb{R}^{p\times m}$, $\mathbf{H} \in \mathbb{R}^{m\times p}$, $\mathbf{I} \in \mathbb{R}^{p\times p}$.

C. State Space Model and Transfer Function

The system and measurement models in Equation (1) and Equation (5) present three states, $p = 3$, and two measurements, $m = 2$. The open-loop SSM representation is obtained combining Equation (7) and Equation (12):

$$\mathbf{x}[n] = \mathbf{A}\mathbf{x}[n-1] + \underbrace{\begin{bmatrix} \alpha_2 & \beta_2 \\ \alpha_1 & \beta_1 \\ \alpha_0 & \beta_0 \end{bmatrix}}_{\mathbf{K}} \tau_{\text{int}} \underbrace{\begin{bmatrix} \delta\phi[n] \\ \delta f[n] \end{bmatrix}}_{\delta\mathbf{z}[n]} \tag{14}$$

$$\underbrace{\begin{bmatrix} \widetilde{\phi}[n] \\ \widetilde{f}[n] \end{bmatrix}}_{\widetilde{\mathbf{z}}[n]} = \mathbf{H}\,\mathbf{A}\,\mathbf{x}[n-1] \tag{15}$$

where $\widetilde{\phi}$ is the estimated carrier phase and $\widetilde{f}$ the estimated carrier Doppler.

The open-loop transfer function is obtained combining the $\mathcal{Z}$-transform of Equation (14) and Equation (15):

$$\widetilde{\mathbf{z}}(z) = \mathbf{H}\,\mathbf{A}\,\left(\mathbf{I} - \mathbf{A}\,z^{-1}\right)^{-1}\,\mathbf{K}\,z^{-1}\,\delta\mathbf{z}(z) \tag{16}$$

Equation (16) is derived as follows:

$$\widetilde{z}_\phi = \sum_{l=0}^{2} \frac{\alpha_l \tau_{\text{int}}^{3-l} z^{-1}}{(1-z^{-1})^{3-l}}\delta\phi + \frac{\beta_l \tau_{\text{int}}^{3-l} z^{-1}}{(1-z^{-1})^{3-l}}\delta f \tag{17}$$

$$\widetilde{z}_f = \sum_{l=0}^{1} \frac{\alpha_l \tau_{\text{int}}^{3-l} z^{-1}}{(1-z^{-1})^{3-l}}\delta\phi + \frac{\beta_l \tau_{\text{int}}^{3-l} z^{-1}}{(1-z^{-1})^{3-l}}\delta f \tag{18}$$

The following relation between carrier Doppler and carrier phase is considered:

$$\delta f = \frac{1-z^{-1}}{\tau_{\text{int}}}\delta\phi \tag{19}$$

Finally, two open-loop transfer functions are observed:

$$H_{\mathrm{o}_\phi}(z) = \sum_{l=0}^{2} \frac{(\alpha_l + \beta_{l-1})\tau_{\text{int}}^{3-l} z^{-1}}{(1-z^{-1})^{3-l}} + \frac{\beta_2}{\tau_{\text{int}}} \tag{20}$$

$$H_{\mathrm{o}_f}(z) = \sum_{l=0}^{1} \tau_{\text{int}} \frac{(\alpha_l + \beta_{l-1})\tau_{\text{int}}^{1-l} z^{-1}}{(1-z^{-1})^{3-l}} + \frac{\beta_1}{1-z^{-1}} \tag{21}$$

These equations show the inter-dependency between PLL and FLL coefficients in the FAP architecture. Figure 1 presents the linear model representation of the LUT-DSKF's state prediction, innovation, and state update for the FAP based on Equation (20).

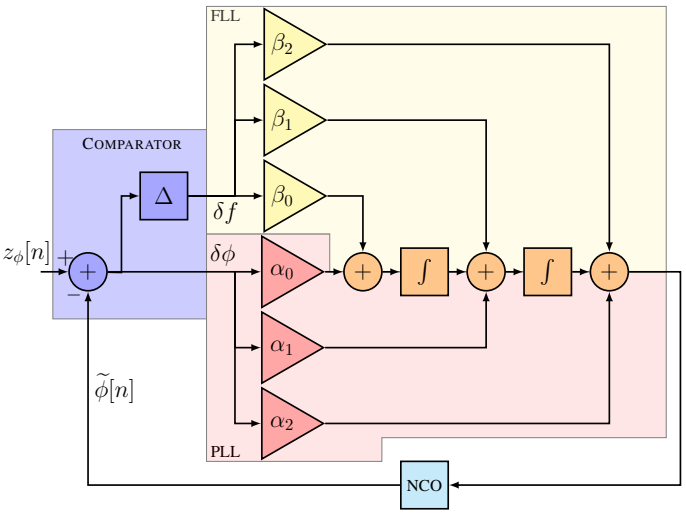

Fig. 1: Linear model of third-order DSKF in FAP.

D. LUT-DSKF

In the steady-state region, the Kalman gains $\mathbf{K}$ converge to a steady-state value given a constant q_a, R_ϕ, and R_f. The expression of the DARE is [29], [30]:

$$\mathbf{P}_{\text{ss}} = \mathbf{A}\,\mathbf{P}_{\text{ss}}\,\mathbf{A}^{\text{T}} + \mathbf{Q} - \mathbf{A}\,\mathbf{P}_{\text{ss}}\,\mathbf{H}^{\text{T}}(\mathbf{H}\,\mathbf{P}_{\text{ss}}\,\mathbf{H}^{\text{T}} + \mathbf{R})^{-1}\mathbf{H}\,\mathbf{P}_{\text{ss}}\,\mathbf{A}^{\text{T}} \quad (22)$$

where $\mathbf{P}_{\text{ss}} \in \mathbb{R}^{3\times 3}$ is the steady-state convergence of the error covariance matrix $\mathbf{P}$. The following is assumed to facilitate the DARE's solution [13]:

$$\mathbf{R}_{i,j} \gg \left(\mathbf{H}\,\mathbf{P}_{\text{ss}}\,\mathbf{H}^{\text{T}}\right)_{i,j} \quad \forall i,j = 1,2 \quad (23)$$

$$R_f \gg R_\phi \quad (24)$$

The approximated solution of $\mathbf{P}_{\text{ss}}$ for a third-order DSKF in the FAP is defined as:

$$\mathbf{P}_{\text{ss}} \approx \mathbf{A}\,\mathbf{P}_{\text{ss}}\,\mathbf{A}^{\text{T}} + \mathbf{Q} - \mathbf{A}\,\mathbf{P}_{\text{ss}}\,\mathbf{H}^{\text{T}}\,\mathbf{R}^{-1}\,\mathbf{H}\,\mathbf{P}_{\text{ss}}\,\mathbf{A}^{\text{T}} \quad (25)$$

$$= \begin{bmatrix} 2q_a^{1/6}R_\phi^{5/6}\tau_{\text{int}} & 2q_a^{1/3}R_\phi^{2/3}\tau_{\text{int}} & q_a^{1/2}R_\phi^{1/2}\tau_{\text{int}} \\ \text{sym.} & 3q_a^{1/2}R_\phi^{1/2}\tau_{\text{int}} & 2q_a^{2/3}R_\phi^{1/3}\tau_{\text{int}} \\ \text{sym.} & \text{sym.} & 2q_a^{5/6}R_\phi^{1/6}\tau_{\text{int}} \end{bmatrix} \quad (26)$$

Applying Equation (26) into Equation (11), and considering the assumption of Equation (23), the steady-state Kalman gain matrix $\mathbf{K}_{\text{ss}}$ is represented as:

$$\mathbf{K}_{\text{ss}} \approx \mathbf{P}_{\text{ss}}\,\mathbf{H}^{\text{T}}\,\mathbf{R}^{-1} \quad (27)$$

$$= \begin{bmatrix} 2(q_a/R_\phi)^{1/6}\tau_{\text{int}} & 2(q_a/R_\phi)^{1/3}\dfrac{R_\phi}{R_f}\tau_{\text{int}} \\ 2(q_a/R_\phi)^{1/3}\tau_{\text{int}} & 3(q_a/R_\phi)^{1/2}\dfrac{R_\phi}{R_f}\tau_{\text{int}} \\ (q_a/R_\phi)^{1/2}\tau_{\text{int}} & 2(q_a/R_\phi)^{2/3}\dfrac{R_\phi}{R_f}\tau_{\text{int}} \end{bmatrix} \quad (28)$$

$$= \begin{bmatrix} 2\gamma\tau_{\text{int}} & 2\gamma^2\dfrac{R_\phi}{R_f}\tau_{\text{int}} \\ 2\gamma^2\tau_{\text{int}} & 3\gamma^3\dfrac{R_\phi}{R_f}\tau_{\text{int}} \\ \gamma^3\tau_{\text{int}} & 2\gamma^4\dfrac{R_\phi}{R_f}\tau_{\text{int}} \end{bmatrix} \quad (29)$$

where γ is the ratio $(q_a/R_\phi)^{1/6}$ in Hertz. The coefficients of the PLL $\{\alpha_0, \alpha_1, \alpha_2\}$ and the coefficients of the FLL $\{\beta_0, \beta_1, \beta_2\}$ are dependant on γ. This parameter determines the time of response of the LUT-DSKF. In the following section, the LBCA is used to adapt γ.

III. LBCA-based LUT-DSKF in FAP

This section describes the architecture of the LBCA-based LUT-DSKF in the FAP tracking scheme. The LBCA updates the loop bandwidth based on a weighted loop-bandwidth dependent difference between estimated dynamics and noise statistics [23]. In previous studies, the LBCA has been implemented in the standard STL [20], [24], the DSKF [14], and the LUT-DSKF [15]. Also, this algorithm has been implemented in the interference mitigation stage to adapt the FLL of an adaptive Notch filter (NF) [31].

The LBCA can update any parameter related to the system's time of response. Equation (29) shows that γ is directly related to all the coefficients of $\mathbf{K}$. Since the loop bandwidth calculation of the LUT-DSKF in a FAP tracking scheme is not trivial to solve, γ is selected to be adapted through the LBCA.

Figure 2 shows the architecture of the modified LBCA to adapt γ. First, the normalized dynamics $D_{\delta\phi}$ of the carrier phase error is calculated:

$$D_{\delta\phi}[n] = \frac{|\mu_{\delta\phi}[n]|}{|\mu_{\delta\phi}[n]| + \sigma_{\delta\phi}[n]} \quad (30)$$

where $|\mu_{\delta\phi}|$ is the absolute mean and $\sigma_{\delta\phi}$ the standard deviation of the carrier phase discriminator's output. Second, the difference between $D_{\delta\phi}$ and a weighting function g is performed:

$$c[n] = g_{\text{Max}}\,D_{\delta\phi}[n] - g[n, \gamma\tau_{\text{int}}] \quad (31)$$

where c is the control value, and g_{Max} is the maximum value of g. The weighting function g depends on the product between the integration time τ_{int} and γ. Finally, the control value updates the current parameter γ:

$$\hat{\gamma}[n] = \gamma[n] + c[n] \quad (32)$$

where $\hat{\gamma}$ is the updated ratio between the steady-state process noise variance q_a and the carrier phase measurement variance R_ϕ. To avoid possible noise instabilities, $\hat{\gamma}$ goes through a Schmitt trigger:

$$\gamma[n+1] = \begin{cases} \frac{6}{5}B_{\text{PLL}_0} & \text{if } n = 0 \\ \hat{\gamma}[n] + \Delta & \text{if } \hat{\gamma}[n] - \gamma[n] \geq \Delta \\ \hat{\gamma}[n] - \Delta & \text{if } \gamma[n] - \hat{\gamma}[n] \leq \Delta \\ \gamma[n] & \text{otherwise} \end{cases} \quad (33)$$

where Δ is the update step set to 0.5 Hz, and B_{PLL_0} is the initial loop bandwidth of the PLL set to 8 Hz.

The selected weighting function g is the one that presented best results in the adaptive PLL architecture [20]:

$$g[n, \gamma\tau_{\text{int}}] = \begin{bmatrix} 0.014 \\ 0.086 \end{bmatrix}^{\text{T}} \begin{bmatrix} \text{Sig}\left(50\left(\gamma\tau_{\text{int}} - 0.06\right)\right) \\ \text{Sig}\left(250\left(\gamma\tau_{\text{int}} - 0.36\right)\right) \end{bmatrix} \quad (34)$$

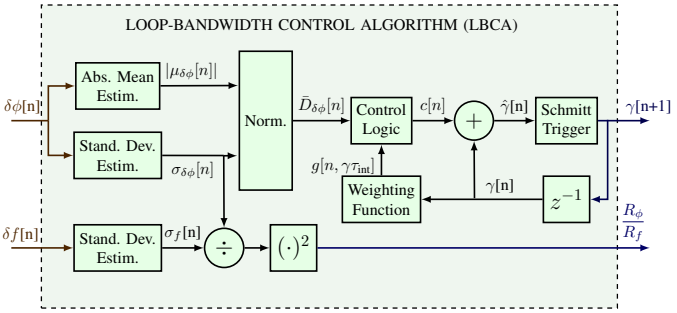

Fig. 2: LBCA architecture used in the LUT-DSKF of a FAP tracking scheme.

where Sig is the Sigmoid function [32]. To reduce the Sigmoid's complexity, the piecewise linear approximation of nonlinearities (PLAN) technique is used [20], [33].

The standard deviation estimation of the frequency discriminator's output is required to calculate the ratio between $R_{\delta\phi}$ and R_f. Due to this operation, the LBCA used in the FAP requires an extra division and multiplication compared to the LBCA implemented in the PLL [15]. The ratio between $R_{\delta\phi}$ and R_f and γ update the steady-state Kalman gains of the FLL $\{\beta_0, \beta_1, \beta_2\}$ (see Equation (29)). Figure 3 presents the architecture of the LBCA-based LUT-DSKF.

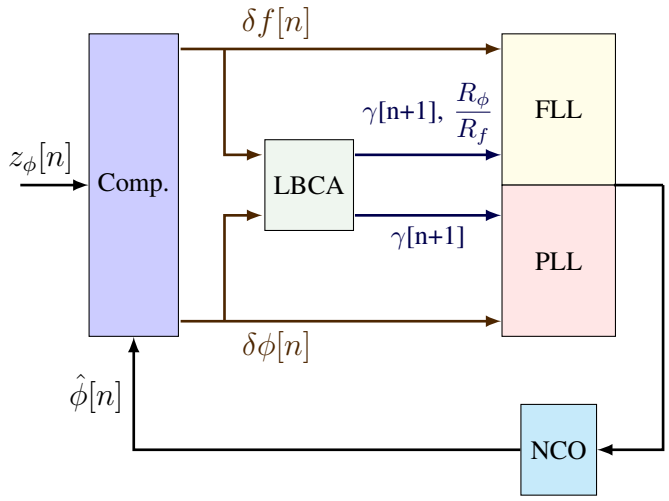

Fig. 3: Adaptive LUT-DSKF of a FAP tracking scheme using LBCA.

IV. Results

This section describes the test setup to evaluate the LBCA-based LUT-DSKF in the FAP and the PLL and presents the static and dynamic tracking performance results. The dataset used to plot the presented results is available on the cloud [34].

A. Evaluation Setup

The evaluation setup is the same as in previous studies [15], [20], [23], [35]. The Spirent GSS9000 radio-frequency constellation simulator (RFCS) generates controlled scenarios at different C/N_0 and signal dynamics levels. The simulator is configured to perform 20 minutes simulations of a specific scenario at different C/N_0 levels. A static scenario and a dynamic scenario are selected to evaluate the adaptive DSKFs. In the static scenario, the Global Positioning System (GPS) L1 C/A signal of satellite vehicle (SV) 4 is selected to evaluate the static tracking performance. For the dynamic scenario, the GPS L1 C/A signal of SV 17 is used to evaluate the dynamic tracking performance. The maximum line-of-sight (LOS) signal dynamics for this dynamic simulated scenario is 8.7 g/s.

The simulator is connected to the GOOSE© platform: a GNSS receiver with an open software interface [25], [36]. The tracking stage of this GNSS receiver is partially implemented in hardware (e.g., correlators and NCO) and software (e.g., discriminators and loop filters). Once the acquisition coarsely estimates the frequency doppler f_d and the code phase τ, the FLL and the DLL try to achieve a more accurate synchronization. The FAP is enabled when a more refined estimate of f_d is achieved. At this stage, the receiver performs the synchronization with the navigation data and the integration time increases to the symbol period. Since the evaluation is done using GPS L1 C/A, the integration time is increased to 20 ms.

The complexity of the LUT-DSKF is similar to the standard STL since the Kalman gain calculations are removed by calculating directly the steady-state values [15]. The LBCA-based LUT-DSKF in the FAP tracking scheme is implemented in software. This section evaluates the LBCA-based third-order LUT-DSKF in the FAP and the PLL tracking architectures.

B. Tracking Performance

The tracking performance $\mathrm{P}_{\text{Tracking}}$ evaluates the tracking of a single SV. This metric is the same as in previous studies [15]:

$$\mathrm{P}_{\text{Tracking}} = (\overline{\sigma}_{\delta\phi} - \sigma_{\text{LB}}) \cdot \lambda \tag{35}$$

where λ is the wavelength of the GNSS signal, $\overline{\sigma}_{\delta\phi}$ is the average of the last ten minutes un-smoothed carrier phase error's standard deviation, and σ_{LB} is the square root Cramér-Rao bound (CRB) of the carrier phase estimation.

The carrier tracking error difference upper threshold, $\mathrm{P}^{\text{th}}_{\text{Tracking}}$ is calculated using the three-sigma rule-of-thumb $\sigma^{\text{th}}_{\delta\phi}$:

$$\mathrm{P}^{\text{th}}_{\text{Tracking}} = \left(\sigma^{\text{th}}_{\delta\phi} - \sigma_{\text{LB}}\right) \lambda \tag{36}$$

For a two-quadrant phase discriminator, $\sigma^{\text{th}}_{\delta\phi}$ has the following value in cycles:

$$\sigma^{\text{th}}_{\delta\phi} = \frac{1}{24} \tag{37}$$

A low value of $\mathrm{P}_{\text{Tracking}}$ indicates good tracking performance. If the measured $\mathrm{P}_{\text{Tracking}}$ is lower than $\mathrm{P}^{\text{th}}_{\text{Tracking}}$, one can ensure a stable tracking and no cycle-slips [1]. The opposite case means that the probability of losing the lock increases.

Figure 4 presents the tracking performance of the LBCA-based LUT-DSKF in the FAP and the PLL. On the one hand, the carrier tracking error difference, $\mathrm{P}_{\text{Tracking}}$, in meters is depicted in Figure 4a. Both adaptive PLL and FAP tracking architectures maintain the tracking lock until 24 dBHz. An improvement bias of the adaptive FAP is observed with respect the adaptive PLL. However, this bias is almost negligible, and it can be concluded that both algorithms perform similarly in the static case. It was expected that the noise addition of the frequency measurement would lead to worse tracking performance of the FAP configuration. Interestingly, the FAP achieves similar tracking performance.

On the other hand, Figure 4b shows the dynamic tracking performance of the adaptive PLL and adaptive FAP. Both architectures maintain the carrier lock until 32 dBHz. At 28 dBHz, both techniques lose the lock, but a lower value of $\mathrm{P}_{\text{Tracking}}$ is observed in the adaptive FAP compared to the

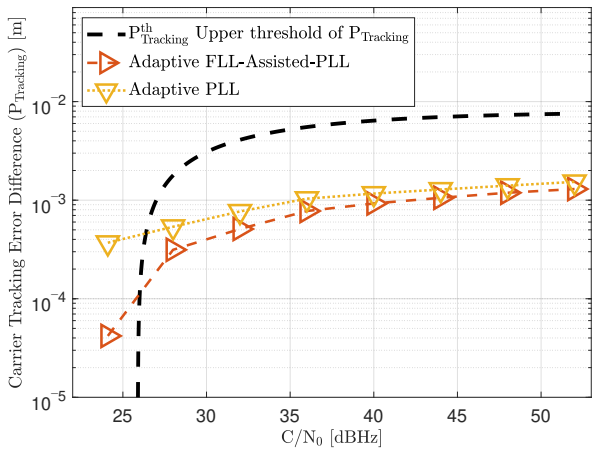

(a) SV G4 in static scenario

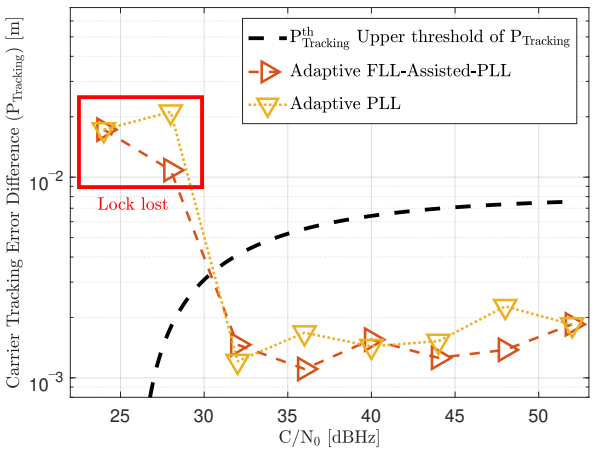

(b) SV G17 in dynamic scenario

Fig. 4: Tracking performance using LBCA-based LUT-DSKF in PLL and FAP tracking schemes.

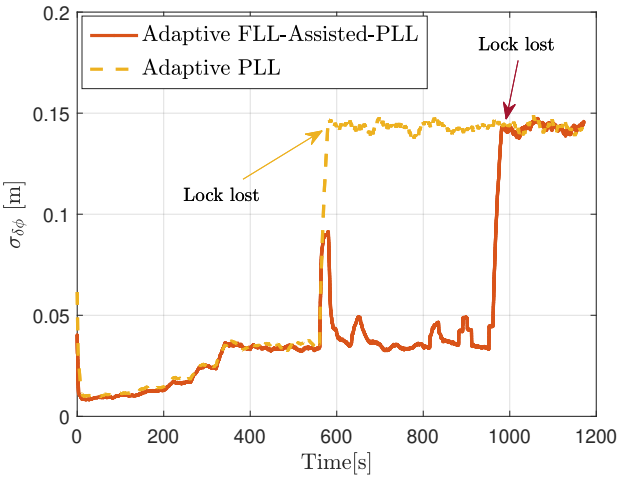

Fig. 5: Standard deviation of phase discriminator's output in dynamic scenario (SV G17) at 28 dBHz.

adaptive PLL. To answer this behaviour, Figure 5 a closer look of the un-smoothed carrier phase error's standard deviation is shown at 28 dBHz. The adaptive PLL loses lock just once dynamics are present, halfway through the simulation, whereas the adaptive FLL resists the high dynamics until the last three minutes of simulation. This observation explains the lower value of $P_{Tracking}$ in the adaptive FAP.

V. Conclusion

This paper evaluates the tracking performance of an adaptive third-order LUT-DSKF in the FAP tracking scheme using a single LBCA. First, the relation of the DSKF in the FAP is analyzed by explaining the system and measurement model, the state space model, and the transfer function. Second, to reduce the complexity of the DSKF, the convergence of the Kalman gains is calculated solving the DARE, deriving the so-called LUT-DSKF. From this simplification, a relationship between Kalman gains based on the ratio parameter γ has been observed (see Equation (29)). Third, the response time of the LUT-DSKF is adapted through γ using the LBCA. Fourth, the static and dynamic tracking performance of the LBCA-based LUT-DSKF in the FAP and in the PLL tracking architectures are presented. The results show that the adaptive FAP mantains a similar static performance compared with the PLL, but achieves a significant improvement in the dynamic performance.

The inter-dependency between FLL and PLL coefficients in a FAP architecture is one of the main findings of this paper. This inter-dependency benefits the implementation of a low complex adaptive technique using a single LBCA. Another important observation is the fact that it is not necessary to set the third coefficient of the FLL, β_2, to zero, as it is usually done. In fact, while deriving the DARE, one can observe that β_2 equals to zero is not the optimal configuration.

An extension of the presented tracking architecture is a LUT-DSKF adapted to a multi-frequency tracking architecture. The use of the LBCA in this architecture cannot only improve the tracking performance in dynamic and noisy scenarios, but it is also a good candidate for multi-path detection and mitigation.

References

[1] E. D. Kaplan and C. J. Hegarty, *Understanding GPS: Principles and Applications*, 2nd ed., ser. Artech House mobile communications series. Artech House, 2006.

[2] D.-J. Jwo, "Optimisation and sensitivity analysis of GPS receiver tracking loops in dynamic environments," in *IEE Proc. - Radar, Sonar and Navigation*, August 2001, pp. 241 – 250.

[3] F. M. Gardner, *Phaselock Techniques*, 3rd ed. Wiley, 2005.

[4] P. F. Driessen, "DPLL bit synchronizer with rapid acquisition using adaptive Kalman filtering techniques," *IEEE Transactions on Communications*, vol. 42, no. 9, pp. 2673–2675, 1994.

[5] A. Gelb and T. A. S. Corporation, *Applied Optimal Estimation*. The MIT Press, 1974.

[6] N. Thacker and A. Lacey, "Tutorial: The likelihood interpretation of the Kalman filter," *Tina Memo*, pp. No. 1996–002, 5 2006.

[7] J. Vilá-Valls, P. Closas, M. Navarro, and C. Fernández-Prades, "Are PLLs dead? A tutorial on Kalman filter-based techniques for digital carrier synchronization," *IEEE Aerospace and Electronic Systems Magazine*, vol. 32, pp. 28 – 45, July 2017.

[8] J. Won, D. Dötterböck, and B. Eissfeller, "Performance comparison of different forms of Kalman filter approaches for a vector-based GNSS signal tracking loop," *NAVIGATION, Journal of the Institute of Navigation*, vol. 57, no. 3, pp. 185–199, Fall 2010. [Online]. Available: https://onlinelibrary.wiley.com/doi/abs/10.1002/j.2161-4296.2010.tb01777.x

[9] J. Won, T. Pany, and B. Eissfeller, "Characteristics of Kalman filters for GNSS signal tracking loop," *IEEE Transactions on Aerospace Electronic Systems*, vol. 48, no. 4, pp. 3671–3681, October 2012.

[10] C. O'Driscoll and G. Lachapelle, "Comparison of traditional and Kalman filter based tracking architectures," in *Proceedings of the European Navigation Conference (ENC 2009)*, 01 2009.

[11] C. O'Driscoll, M. Petovello, and G. Lachapelle, "Choosing the coherent integration time for Kalman filter based carrier phase tracking of GNSS signals," *GPS Solutions*, vol. 15, pp. 345–356, 10 2011.

[12] X. Tang, G. Falco, E. Falletti, and L. L. Presti, "Theoretical analysis and tuning criteria of the Kalman filter-based tracking loop," *GPS Solut.*, vol. 19, pp. 489–503, 2014.

[13] ——, "Complexity reduction of the Kalman filter-based tracking loops in GNSS receivers," *GPS Solut.*, vol. 21, no. 2, p. 685–699, 4 2017. [Online]. Available: https://doi.org/10.1007/s10291-016-0557-6

[14] I. Cortés, P. Marín, J. R. van der Merwe, E. Simona Lohan, J. Nurmi, and W. Felber, "Adaptive techniques in scalar tracking loops with direct-state kalman-filter," in *2021 International Conference on Localization and GNSS (ICL-GNSS)*, 2021, pp. 1–7.

[15] I. Cortés, J. R. van der Merwe, E. S. Lohan, J. Nurmi, and W. Felber, "Performance evaluation of adaptive tracking techniques with direct-state Kalman filter," *Sensors*, vol. 22, no. 2, 2022. [Online]. Available: https://www.mdpi.com/1424-8220/22/2/420

[16] J. W. Won and B. Eissfiller, "A tuning method based on signal-to-noise power ratio for adaptive PLL and its relationship with equivalent noise bandwidth," *IEEE Communication Letters*, vol. 17, no. 15, pp. 393 – 396, January 2013.

[17] J.-H. Won, "A novel adaptive digital phase-lock-loop for modern digital GNSS receivers," *IEEE Communication Letters*, vol. 18, no. 1, pp. 46–49, January 2014.

[18] J. Vilà-Valls, P. Closas, and C. Fernández-Prades, "On the identifiability of noise statistics and adaptive KF design for robust GNSS carrier tracking," in *2015 IEEE Aerospace Conference*, Big Sky, MT, USA, 2015, pp. 1–10.

[19] J. A. López-Salcedo, J. A. D. Peral-Rosado, and G. Seco-Granados, "Survey on robust carrier tracking techniques," *IEEE Communication Surveys & Tutorials*, vol. 12, no. 2, pp. 670 – 688, January 2014.

[20] I. Cortés, J. R. van der Merwe, J. Nurmi, A. Rügamer, and W. Felber, "Evaluation of adaptive loop-bandwidth tracking techniques in GNSS receivers," *Sensors*, vol. 21, no. 2, 2021. [Online]. Available: https://www.mdpi.com/1424-8220/21/2/502

[21] J. Duník, O. Straka, O. Kost, and J. Havlík, "Noise covariance matrices in state-space models: A survey and comparison of estimation methods—part i," *International Journal of Adaptive Control and Signal Processing*, vol. 31, no. 11, pp. 1505–1543, 2017. [Online]. Available: https://onlinelibrary.wiley.com/doi/abs/10.1002/acs.2783

[22] P. Bolla, "Advanced tracking loop architectures for multi-frequency GNSS receiver," Ph.D. dissertation, Tampere University of Technology, Finland and Samara University, Russia, 12 2018.

[23] I. Cortes, J. R. Van der Merwe, A. Rügamer, and W. Felber, "Adaptive loop-bandwidth control algorithm for scalar tracking loops," in *Proceedings of IEEE/ION PLANS*, 2020.

[24] I. Cortés, S. Urquijo, M. Overbeck, W. Felber, L. Agrotis, V. Mayer, E. Schönemann, and W. Enderle, "Robust tracking strategy for modern GNSS receivers in sounding rockets," in *ESA Workshop on Satellite Navigation User Equipment Technologies (NAVITEC)*, April 2022.

[25] M. Overbeck, F. Garzia, A. Popugaev, O. Kurz, F. Forster, W. Felber, A. S. Ayaz, S. Ko, and B. Eissfeller, "GOOSE - GNSS receiver with an open software interface," in *Proceedings of the 28th International Technical Meeting of The Satellite Division of the Institute of Navigation (ION GNSS 2015)*, September 2015.

[26] A. Lasota, *Chaos, fractals, and noise : stochastic aspects of dynamics / Andrzej Lasota, Michael C. Mackey.*, 2nd ed., ser. Applied mathematical sciences ; v. 97. New York: Springer-Verlag, 1994.

[27] S. Aguirre, W. Hurd, R. Kumar, and J. Statman, "A comparison of methods for DPLL loop filter design," Jet Propulsion Laboratory, Telecommunications and Data Acquisition Progress Report 42-79, November 1986.

[28] E. I. Jury, *Theory and application of the Z-transform methods*. New York: Wiley, 1964.

[29] G. Einicke, *Smoothing, filtering and prediction: estimating the past, present and future*. InTechOpen, 01 2012.

[30] R. G. Brown and P. Y. C. Hwang, *Introduction to random signals and applied Kalman filtering: with MATLAB exercises and solutions; 3rd ed.* New York, NY: Wiley, 1997. [Online]. Available: https://cds.cern.ch/record/680442

[31] J. R. van der Merwe, I. Cortés, F. Garzia, E. S. Lohan, J. Nurmi, and W. Felber, "Resilient interference mitigation with adaptive frequency locked loop based adaptive notch filtering," in *2021 Navigation*, 11 2021, pp. 1–18.

[32] P. Domingos, *The Master Algorithm: How the Quest for the Ultimate Learning Machine Will Remake Our World*. USA: Basic Books, Inc., 2018.

[33] H. Amin, K. Curtis, and B. Hayes-Gill, "Piecewise linear approximation applied to nonlinear function of a neural network," in *IEE Proceedings - Circuits, Devices and Systems*, vol. 144, 1997, pp. 313 – 317.

[34] "Robust Tracking Techniques Dataset using GOOSE Receiver," https://owncloud.fraunhofer.de/index.php/s/LGoWPVtV5xbQ9mB.

[35] I. Cortés, J. A. Iñiguez de Gordoa, J. R. van der Merwe, A. Rügamer, and W. Felber, "Performance and complexity comparison of adaptive loop-bandwidth tracking techniques," in *2020 International Conference on Localization and GNSS (ICL-GNSS)*, 2020, pp. 1–7.

[36] J. Seybold, "GOOSE: Open GNSS Receiver Platform," TeleOrbit GmbH, Tech. Rep., 2020, available Online: https://teleorbit.eu/en/satnav/.